Hindawi Publishing Corporation
BioMed Research International
Volume 2014, Article ID 625095, 13 pages
http://dx.doi.org/10.1155/2014/625095

Review Article

Current Opportunities and Challenges of Magnetic Resonance Spectroscopy, Positron Emission Tomography, and Mass Spectrometry Imaging for Mapping Cancer Metabolism *In Vivo*

Gigin Lin[1,2,3] and Yuen-Li Chung[4]

[1] *Department of Radiology, Chang Gung Memorial Hospital at Linkou, Chang Gung University, 5 Fuhsing Street, Guishan, Taoyuan 333, Taiwan*
[2] *Molecular Imaging Center, Chang Gung Memorial Hospital at Linkou, Chang Gung University, 5 Fuhsing Street, Guishan, Taoyuan 333, Taiwan*
[3] *Metabolomics Core Laboratory, Chang Gung Memorial Hospital at Linkou, Chang Gung University, 5 Fuhsing Street, Guishan, Taoyuan 333, Taiwan*
[4] *The Institute of Cancer Research and Royal Marsden Hospital, CRUK Cancer Imaging Centre, Downs Road, Sutton, Surrey SM2 5PT, UK*

Correspondence should be addressed to Yuen-Li Chung; yuen-li.chung@icr.ac.uk

Received 19 October 2013; Revised 6 January 2014; Accepted 19 January 2014; Published 3 March 2014

Academic Editor: Tzu-Chen Yen

Copyright © 2014 G. Lin and Y.-L. Chung. This is an open access article distributed under the Creative Commons Attribution License, which permits unrestricted use, distribution, and reproduction in any medium, provided the original work is properly cited.

Cancer is known to have unique metabolic features such as Warburg effect. Current cancer therapy has moved forward from cytotoxic treatment to personalized, targeted therapies, with some that could lead to specific metabolic changes, potentially monitored by imaging methods. In this paper we addressed the important aspects to study cancer metabolism by using image techniques, focusing on opportunities and challenges of magnetic resonance spectroscopy (MRS), dynamic nuclear polarization (DNP)-MRS, positron emission tomography (PET), and mass spectrometry imaging (MSI) for mapping cancer metabolism. Finally, we highlighted the future possibilities of an integrated *in vivo* PET/MR imaging systems, together with an *in situ* MSI tissue analytical platform, may become the ultimate technologies for unraveling and understanding the molecular complexities in some aspects of cancer metabolism. Such comprehensive imaging investigations might provide information on pharmacometabolomics, biomarker discovery, and disease diagnosis, prognosis, and treatment response monitoring for clinical medicine.

1. Introduction

Cancer is known to have unique metabolic features [1]. Knowledge of cancer metabolism can be applied not only for early detection and diagnosis of cancer, but also in the evaluation of tumor response to medical interventions and therapies [2]. The first characterized phenotype observed in cancer cells is the Warburg effect [3], which describes a shift from energy generation through oxidative phosphorylation to energy generation through anaerobic glycolysis, even under normal oxygen concentrations. Anaerobic glycolysis produces only two ATPs per glucose and is less efficient than oxidative phosphorylation [4, 5]. Cancer cells require high-energy demand to support cell growth and proliferation; therefore cancer cells have increased glucose uptake, glycolytic activity, and lactate production and decreased mitochondrial activity, low bioenergetic status, and aberrant phospholipid metabolism [6, 7]. Several important oncogenes involved in the development and progression of common human cancers have also been found to regulate glycolysis. For example, unregulated activity of the serine/threonine kinase Akt has been shown to increase glucose uptake of tumor cells as well as increase resistance to apoptosis [8–10]. The oncogene *c-myc*, a transcription factor, controls and activates numerous glycolytic genes (e.g., hexokinase 2, enolase, and lactate dehydrogenase A) [11, 12]. Oncogenic *ras* is an important protein

that controls signaling pathways for cell growth, regulation, and malignancy transformation [13] and it has been seen to increase the concentration of fructose-2,6,-bisphosphate (F2, 6BP), which is an allosteric activator of phosphofructo1-kinase, and it catalyzes the phosphorylation of fructose-6-phosphate to fructose-1,6-bisphosphate [14]. Recent advances have established further links between cancer metabolism and genetic alterations in *p53* [15], AMPK [16], PI3K [17, 18] and HIF [19].

There are growing interests in developing therapies that target important signaling pathways (e.g. PI3K [18] and MAPK [20]) and transcription factors (e.g. HIF-1 [21]) and inhibit upregulated enzymes (e.g. pyruvate dehydrogenase kinase (PDK) [22] and choline kinase [23]) and metabolite transporters (e.g. glucose transporter (Glut1) [24] and monocarboxylate transporter-1 (MCT-1) [25]). Those targeted therapies might alter cancer metabolism, and the changes in endogenous metabolites in cancer cells might be detected even before changes in tumor sizes [26–28]. Imaging methods are needed to detect early metabolic changes in cancer following treatment and these imaging readouts could be useful for monitoring the response to therapies [29, 30].

Tumor heterogeneity and its adaptations to microenvironment are important factors that could affect the effectiveness of cancer treatment; hence, the ability to image and spatially map the heterogeneity of metabolism within a tumor will be very useful for planning the treatment regime. Intratumoral heterogeneity and branched evolution are recently revealed in multiple spatially separated samples obtained from primary renal carcinomas and associated metastatic sites by using genome sequencing [31]. In addition, the metabolic heterogeneity is not only attributed to genetic alteration but is also an adaptation to hypoxic tumor microenvironment. Glycolysis confers a significant growth advantage by producing the required metabolites for cancer growth [27, 32–34], as lactate can be used by oxygenated cancer cells as oxidative fuel [35], in order to spare the glucose for the more anoxic cells in the center of the tumor [36]. This cooperation between hypoxic and normoxic tumor cells optimizes energy production and allows cells to adapt efficiently to their environmental oxygen conditions [37, 38].

Conventionally, nuclear magnetic resonance (NMR) spectroscopy [67] and mass spectrometry (MS) [68] can be used separately or in combination to provide overlapping yet complementary data to evaluate cancer [69–72]. MS have high sensitivity but the samples required prior separations using gas- or lipid-chromatography. NMR has a lower sensitivity than MS but it can measure all the detectable molecules in the sample simultaneously without the need to prior separation, cancelling out the quantification errors within the method [69]. Although analyses of biopsies with many metabolites correlated with disease aggressiveness [73], the conventional metabolomic experiments using a single biopsy of small tumor or extracting metabolites from relatively large tissue areas do not provide the spatial information of the metabolites and multiple biopsies or biopsy of normal tissue counterpart; for comparison is not feasible in routine clinical practice. Hence, noninvasive imaging would be a useful solution for spatial mapping of metabolites. The potential imaging techniques reviewed in this paper include, but are not limited to, magnetic resonance spectroscopy (MRS), dynamic nuclear polarization (DNP) MRS, positron emission tomography (PET), and mass spectrometry imaging (MSI) for tissue characterization. Table 1 summarizes the advantages, disadvantages, and clinical applications of each imaging technique.

2. Magnetic Resonance Spectroscopy (MRS)

Magnetic resonance spectroscopy (MRS) is a technique that can be used in preclinical and clinical settings to study cancer metabolism [74]. It is based on nuclei such as ^{1}H, ^{31}P and, ^{13}C that possess the property of magnetic spin. When they are placed in a magnetic field, these nuclei become aligned or opposed to the external magnetic field. Many of the nuclei are flipped into the other magnetic state when a radiofrequency pulse is applied, and the differences in the populations between these two magnetic energy states are detected as a radio wave as the system returns to equilibrium. The strength of this local field depends on the electronic environment around the nucleus. Different chemical structures possess different electronic environments and lead to nuclei resonating at slightly different frequencies. These frequencies are termed as chemical shifts, which are expressed as the dimensionless units, parts per million (ppm), in the spectrum and represent the metabolites of the measured sample [75]. Additional magnetic field gradients cause nuclei at different locations to precess at different speeds, which allows spatial information to be recovered using Fourier analysis of the measured signal [75]. By spatially encoding chemical shift information, one can generate MRS imaging by obtaining signals at different chemical shifts. This can be achieved by frequency selective radiofrequency pulses, as in stimulated echo acquisition mode (STEAM) [76] and point-resolved spectroscopy (PRESS) [77] in proton (^{1}H)-MRS, or by excitation and subsequent subtraction of unwanted signals, as in image selective *in vivo* spectroscopy (ISIS) technique [78] in phosphorus (^{31}P)-MRS. In addition, multivoxel spectroscopy, such as chemical shift imaging (CSI) [79], can collect spectroscopic data from multiple adjacent voxels in a single measurement.

The clinical use of spectroscopy as an adjunct to MRI has expanded dramatically over the past decades because of technical advances in hardware and pulse sequence design that have improved the spatial and temporal resolution of spectral data. Nowadays most clinical MR scanners have routine sequences for ^{1}H-MRS measurements, providing a wide range of metabolic and functional information integrated with complementary MRI localization. Metabolites commonly detected in clinical ^{1}H-MRS include N-acetyl-aspartate (NAA) in the normal brain tissue [39] and citrate in the normal prostate [40], and their levels decrease once being replaced by tumor. MRS detection of total choline signal has been used to diagnose and monitor breast [41], brain [42], and prostate cancers [44] and for monitoring the response to anticancer therapy [23, 72, 80]. In addition,

Table 1: Comparison of major imaging techniques for studying cancer metabolism.

Imaging techniques	Advantages	Disadvantages	Clinical applications	References
Magnetic resonance spectroscopy (MRS)	(i) Widely used medical imaging technique (ii) Ability to assess multiple metabolites in one measurement (iii) No radiation concern	(i) It has relatively long acquisition time (ii) Data processing is not routine in the clinic (iii) Lack of familiarity with clinicians	Brain, head and neck, prostate, breast, and cervix	[39–46]
Dynamic nuclear polarization- (DNP-) MRS	(i) Signal enhancements of over 10,000-fold of magnitude for stable isotope carbon-13 (^{13}C) enriched compounds (ii) Simultaneous detection of multiple hyperpolarized molecules allowed several metabolic pathways to be probed at the same time (iii) No radiation concern (iv) Short acquisition time (v) Real-time observation of not only the uptake of the targeted molecule but also its flux to produce downstream metabolic products	Hyperpolarized 13C-labelled substrates have very short half-life (in tens of seconds)	Prostate	[47]
Positron emission tomography (PET)	(i) Widely used in clinical applications (ii) High sensitivity	(i) Not all tumors show a significant increase in metabolic activity on FDG-PET imaging (ii) Difficult to evaluate malignant lesions in tissues that physiologically take up FDG (such as the central nervous system) or excrete FDG (such as the kidneys and bladder) or differentiate between inflammation and cancer (iii) Radiation concern (iv) It measures perfusion and accumulation of a tracer and does not differentiate between metabolites containing the radionuclide or tracer per se	Oral cancer, lymphoma, melanoma, lung cancer, esophageal cancer, and colorectal cancer Cervical Ovarian Pancreas Prostate	[48–57]
Mass spectrometry imaging (MSI)	(i) Highly sensitive (ii) It can be used to investigate both identified and unidentified molecules in spatial localized areas without any need for labeling or contrasting agents	Analytical technique of tissue section, not noninvasive imaging	Brain, oral, lung, breast, gastric, pancreatic, renal, ovarian, and prostate cancer	[58–66]

in vivo ^{1}H-MRS also detects signals from lipid metabolism-related compounds, such as the methylene ($-CH_2$) signal at 1.3 ppm and the methyl (CH_3) signal at 0.9 ppm [81], which originate from the fatty acyl chains of the cytoplasmic mobile lipids and not from the membrane lipids [82]. Significantly higher levels of lipid have been detected in high-grade human gliomas when compared to low-grade gliomas [81], and these changes are associated with apoptosis, necrosis, or lipid droplet formation [83–85].

^{31}P-MRS could provide information on tumor bioenergetics and metabolites such as nucleoside triphosphates (NTPs), phosphocreatine (PCr), and inorganic phosphate (Pi). The production of high-energy phosphates such as NTP and PCr depends on the availability of glucose and oxygen (which are delivered to the tumors through blood vessels), and is determined by diffusion distances and local oxygen consumption rates. Therefore, in addition to blood flow parameters measured by DCE-MRI or perfusion CT, ^{31}P-MRS provides an opportunity to monitor downstream biochemical reactions following reduced blood flow in hypoxic regions [85] and is useful in detecting changes in tumor reoxygenation during radiation therapy [86] as well as altered tissue pH level (measured by the Pi chemical shift changes) [87]. ^{31}P-MRS also measures phospholipid metabolites, such as phosphomonoester and phosphodiester in tumor, which in turn could inform on membrane turnover and tumor response following therapies [23, 72, 81].

MRS can also directly measure the pharmacokinetics of drugs that present at relatively high concentrations in the tumor. Most *in vivo* studies on MR pharmacokinetic

measurements of tumors employ fluorinated drugs, such as [5-^{19}F]-fluorouracil (5-FU) and its prodrug, as detected by ^{19}F MRS [88, 89], because ^{19}F MRS provides relatively high sensitivity combined with low background signal. Successful image-guided delivery of a prodrug enzyme, bacterial cytosine deaminase (bCD), which converts nontoxic [5-^{19}F]-fluorocytosine (5-FC) to 5-FU, was recently reported in preclinical studies [90].

Relative to conventional MRI, MRS has lower sensitivities and requires much longer acquisition times and more complex data processing, and with clinicians unfamiliar with the technique, these factors continue to limit the application of MRS in the clinical setting. Currently, there are methodologies that optimize the combined signals from multielement coil arrays to improve detection of low concentration metabolites in MRS [91], in order to improve its sensitivity and spectral resolution. In addition, the availability of higher field strength MR systems and novel techniques such as dynamic nuclear polarization hyperpolarization (DNP) can reduce some of these limitations.

3. DNP-MRS

DNP is a novel imaging technique which uses specialized instrumentation to provide signal enhancements of over 10,000-folds of magnitude for stable isotope carbon-13 (^{13}C) enriched compounds [92]. Simultaneous detection of multiple hyperpolarized molecules allow several metabolic pathways to be probed at the same time [93, 94], and this enhanced ^{13}C signal allows the distribution of hyperpolarized ^{13}C-labeled molecules within the tumor tissue to be visualized [95]. [1-^{13}C]Pyruvate has been the most widely studied substrate to date because of its central role in cellular metabolism. [1-^{13}C]Pyruvate also has relatively longer $T1$ relaxation time and rapid transport into the cells for subsequent metabolism [96]. Hyperpolarized [1-^{13}C]pyruvate has been used to study the real-time flux of pyruvate to lactate noninvasively following anticancer therapies in xenograft models [97–101]. The first clinical trial of DNP-MRS has recently demonstrated the use of hyperpolarized [1-^{13}C]pyruvate to examine prostate cancer metabolism in human [47] (Figure 1), and it paves the way to rapid translation of this exciting technology to clinical research and perhaps clinical practice [96]. Previously, the data analysis to obtain the apparent rate of pyruvate to lactate exchanges following the [1-^{13}C]pyruvate DNP-MRS experiment is quite complex, as it requires the fitting of the data to a mathematical model [102]. A much simpler method to analyze this type of data has been developed recently [103], which will improve the ease of use of this methodology in studying cancer metabolism. In addition to pyruvate, extracellular pH has been measured in lymphoma xenografts by using hyperpolarized $H^{13}CO_3^-$ and pH images were obtained by measuring the $H^{13}CO_3^-/{}^{13}CO_2$ ratio in each imaging voxel [104]. [1, 4-^{13}C$_2$]Fumarate is potentially a useful agent for detecting treatment response in tumors because the production of labeled malate was shown to be an indicator of necrotic cell death [105].

4. Positron Emission Tomography (PET)

Positron emission tomography (PET) is a nuclear medical imaging technique that produces three-dimensional imaging data of functional processes in the body. The system detects pairs of gamma rays emitted indirectly by positron-emitting radionuclide tracers, to provide functional or metabolic information in PET imaging [107]. When combined with X-ray computed tomography (CT), PET/CT imaging can provide both molecular information and anatomic localization. ^{18}F-fluorodeoxyglucose (FDG) PET is by far the most successfully used imaging technique to study glucose uptake in tumors *in vivo*. After intravenous injection, ^{18}F-FDG is transported across the cell membrane by glucose transporters and metabolized to ^{18}F-FDG-6-phosphate by hexokinase [108]. In contrast to the complex metabolic fate of glucose-6-phosphate from glucose, ^{18}F-FDG-6-phosphate cannot be further metabolized in the glycolytic pathway because the fluorine atom at the C_2 position prevents ^{18}F-FDG-6-phosphate from downstream catabolism. This leads to steady accumulation of ^{18}F-FDG-6-phosphate in metabolically active cells such as cancer [109].

Over the past decade, ^{18}F-FDG PET/CT has become a routine clinical test for staging and restaging of a variety of malignant tumors, including head and neck cancer, lymphoma, colorectal, cervical cancer (Figure 2, [56]), and many other solid organ cancers [48], with a sensitivity of about or above 90% [110]. There is considerable evidence that the reduction of ^{18}F-FDG uptake is caused by a loss of viable tumor cells following chemo- and radiotherapy [111]. However, the close relationship between various oncogenic signaling pathways and tumor glucose metabolisms suggests that the drugs targeting these signal transduction pathways may have a more direct effect on cellular glucose metabolism. For example, decreased ^{18}F-FDG uptakes were found in patients with gastrointestinal stromal tumors (GIST) within hours following treatment with the c-Kit inhibitor imatinib [50, 51]. Rapid reduction in ^{18}F-FDG uptakes was also observed in patients with non-small cell lung cancer treated with EGFR kinase inhibitor gefitinib [52].

Although ^{18}F-FDG is widely used in clinical applications, not all tumor types show a significant increase in metabolic activity on ^{18}F-FDG PET imaging, for example, in prostate, neuroendocrine, and hepatic tumors [48]. Furthermore, it is difficult to evaluate malignant lesions in organs that normally take up (such as the central nervous system) or excrete FDG (such as the kidneys, urinary bladder, and prostate) or to differentiate between inflammation and cancer. Therefore, other PET tracers in addition to FDG have been developed for oncological studies [30], either for clinical use or at different stages of clinical evaluation. These compounds include ^{11}C-acetate (a precursor of membrane fatty acids) in prostate cancer [112], ^{11}C-methionine (a precursor of S-adenosylmethionine, which is required for polyamine synthesis) in brain tumor [113], ^{18}F-choline (a substrate of choline kinase in choline metabolism) in prostate cancer [114], and ^{18}F-3′-fluoro-3′-deoxy-L-thymidine (^{18}F-FLT) (a substrate of thymidine kinase [TK-2] in DNA synthesis

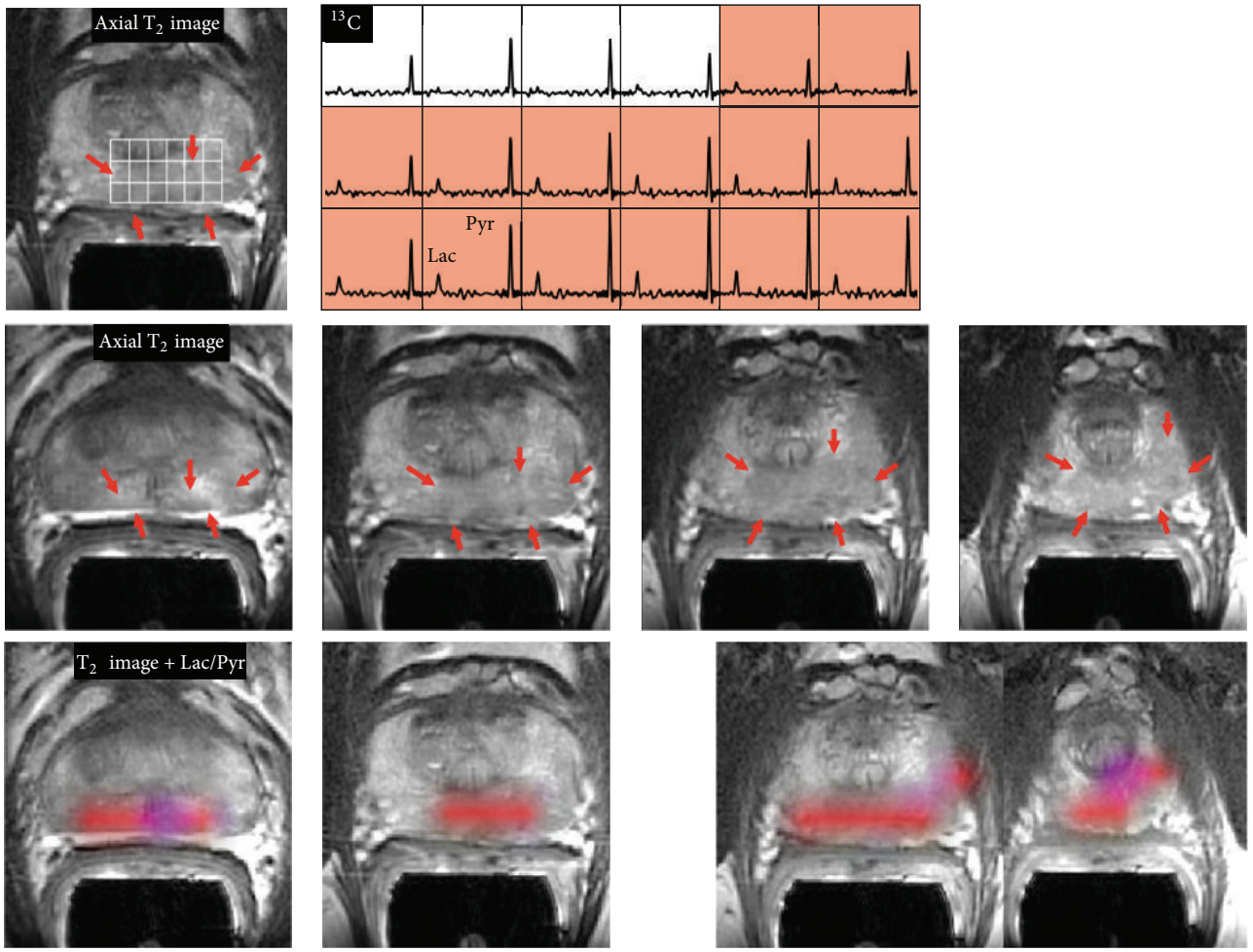

Figure 1: 3D [1-^{13}C]Pyruvate dynamic nuclear hyperpolarization magnetic resonance spectroscopy (DNP-MRS) imaging in a patient with prostate cancer. The upper panel shows an axial T2-weighted images and corresponding spectral array with the area of putative tumor highlighted by pink shading. A region of tumor was observed on the T2-weighted images (red arrows). A region of relatively high hyperpolarized [1-^{13}C]lactate was observed in the same location as the abnormalities that had been observed on the multiparametric 1H staging exam. The lower panels show axial T2 images with and without metabolite overlays for different axial slices from the same patient. The colored regions in these overlays have a ratio of [1-^{13}C]lactate/[1-^{13}C]pyruvate ≥0.2. These demonstrated a large volume of bilateral cancer. Reprinted with permission from [106]. Copyright 2013 American Association for the Advancement of Science.

and a specific marker of cell proliferation) [115]. Efforts are also made to improve detection and measurement of low level metabolized ^{18}F tracer from the ^{18}F-labeled pyrimidine nucleoside analogues [116].

4.1. Comparison of PET and DNP-MRS. An advantage of DNP-MRS is that it does not have radiation concern that is commonly associated with PET. Although both PET and DNP-MRS can measure the uptake of labeled substrates in real-time, another key advantage of DNP-MRS is that both the injected substrate and its metabolic products can be detected and followed in real-time, allowing the observation of not only the uptake of the targeted molecule but also its downstream metabolic products [96]. In contrast, PET measures perfusion and accumulation of a tracer, but does not differentiate between metabolites containing the radionuclide or tracer per se.

The most notable limitation of DNP-MRS imaging is the very short half-life (in tens of seconds) of the hyperpolarized ^{13}C-substrates, which is affected by the substrates' $T1$ value and the field strength of the MR scanner (lower field strength MR scanner improves the half-life of the hyperpolarized substrates) [96]. The hyperpolarized state decreases to its equilibrium value with a time constant according to the spin lattice relaxation time $T1$. $T1$ relaxation times are dependent on the nucleus but are also sensitive to a host of other factors including the applied field, the location in a molecule, molecular structure and motion, and the chemical environment.

In general, PET is much more sensitive than DNP-MRS [117]. PET tracers can be detected in the nano- to picomolar

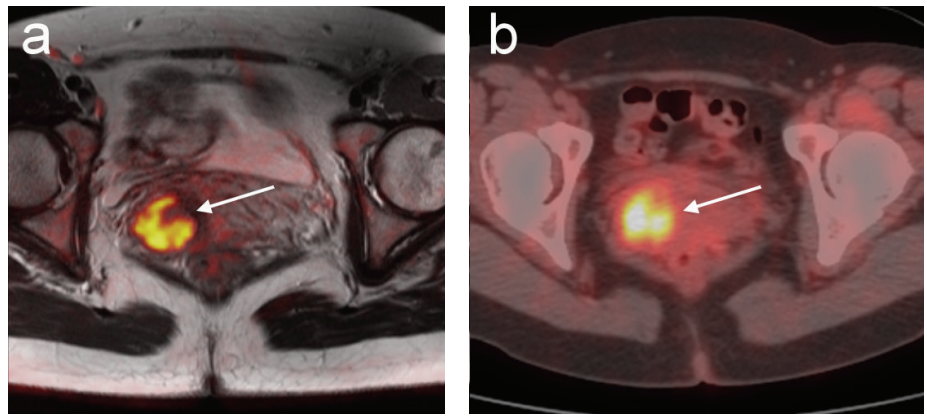

(a) (b)

Figure 2: An example of PET/CT and MRI in the female pelvis. A 43-year-old female patient with a primary well-differentiated adenocarcinoma of the uterine cervix. Primary cervical tumor is highlighted (arrow) and well correlated in (a) diffusion-weighted MRI and (b) 18F-FDG PET/CT. Reprinted with permission from [56]. Copyright 2008 Springer-Verlag.

range [118]; whereas DNP-MRS sensitivity is still in the millimolar range. Therefore, DNP molecules are injected at concentrations that greatly exceed physiologic levels (e.g., 15–28 mmoles of pyruvate in mouse models [97, 119]), whereas PET-labeled molecules can be administered at concentrations that are unlikely to perturb normal metabolism. Although hyperpolarized [1-^{13}C]pyruvate increases the sensitivity of MR imaging, signal-to-noise ratio constraints still exist for spatial and temporal resolution of ^{13}C DNP-MRS, especially relative to PET, emphasizing the need for further development of MR methodology [96].

4.2. Potential of Simultaneous PET/MRS. The integrated PET/MRI system could offer potential in the management of cancer, with prostate, head/neck, and breast cancers among the primary indications for PET/MRI [120]. The benefit of integrating PET and MRI might not only result in improved sensitivity and spatial resolution, but also allow the specific sets of metabolic events to be examined at the same time [121]. In a preclinical murine glioma model, advancing tumor proliferation caused an increase in ^{11}C-choline uptake as measured by PET, while gliosis and inflammation accounted for a high peritumoral total choline signal in MRS [122]. A decrease in ^{18}F-FDG PET and changes in phosphomonoesters by ^{31}P-MRS were associated with decreases in hexokinase II and Glut1 expression in HER2 expressing breast tumor xenografts and responding to trastuzumab treatment [123]. These studies exemplified that PET/MRS could be used to monitor treatment response and could provide unique information on drug biodistribution, targeting, and metabolism and serve as surrogate pharmacokinetics/pharmacodynamics (PK/PD) markers [124].

Although clinical evidence of simultaneous PET and MRS measurement is not available at present, previous reports based on the correlation of PET and MRS have demonstrated the potential usefulness of integrated PET/MRS. A significant positive correlation was found between tumor total choline concentration by ^{1}H-MRS and total lesion glycolysis measured by ^{18}F-FDG PET before treatment in head and neck cancer patients [125]. For primary staging in prostate cancer patients, ^{1}H-MRS was reported to improve the sensitivity of ^{11}C-choline PET/CT in localizing tumor in the prostate gland and achieved up to 97% of overall accuracy [126]. Combined ^{1}H-MRS and DCE-MRI have improved the sensitivity of ^{18}F-choline PET/CT from 62% to 92% in identifying local prostate cancer recurrence, particularly in patients with low biochemical progression after surgical treatment [127]. For breast cancer patients with an invasive ductal carcinoma of 1.5–3 cm in size, the total choline level in tumors measured by ^{1}H-MRS was highly correlated with the standardized ^{18}F-FDG uptake value obtained by PET/CT, and these measurements were also supported by the histologic prognostic parameters (nuclear grade, estrogen receptor status, and triple-negative lesion status) [128]. The sensitivity and specificity of total choline level by ^{1}H-MRS for detecting breast cancer were 83% and 85%, respectively, and both values could be as high as 92% after technical exclusions [129].

Whether the simultaneous collection of MRS data together with PET/MRI will improve diagnosis of brain tumor remained unclear. However, evidence shows that by using choline/creatine ratio > 1.5 as a threshold, the addition of ^{1}H-MRS could marginally increase the sensitivity of contrast-enhanced MRI, from 86% to 100% (P = .79), without altering the specificity (67%) [130]. In addition, by using cutoff points of NAA/Cho $\leq$ 0.61 on ^{1}H-MRS and relative cerebral blood volume (rCBV) $\geq$ 1.50 (corresponding to diagnosis of the tumors), a sensitivity of 72% and specificity of 91% in differentiating tumors from nonneoplastic lesions have been achieved [131]. The distinction of MRS between recurrent tumor and radiation necrosis in brain tumor using the Cho/NAA ratio could be made with 85% sensitivity and 69% specificity [132].

Hepatocyte-specific (gadoxetic acid) enhanced MRI is a powerful diagnostic tool for hepatocellular carcinoma (HCC) [133], with sensitivity of about 81–90% for lesion size < 2 cm [134, 135]. For the detection of HCC, ^{18}F-FDG PET/CT has a sensitivity of only around 64%–68%, which can be improved by using ^{11}C-acetate [136] and ^{18}F-fluorocholine [137] tracers, with reported sensitivity rising to 84% and 88%, respectively. Direct comparison of diagnostic accuracy of ^{11}C-acetate or ^{18}F-fluorocholine PET/CT versus hepatocyte-specific MRI on liver tumors would be of great interest; this area of research is still under investigation. Menzel et al. recently reported a multimodal *in vivo* assessment of glucose metabolism in HCC tumors using hyperpolarized [1-^{13}C]pyruvate DNP-MRS and ^{18}F-FDG PET [138]. The increased [1-^{13}C]lactate signals in the tumor is correlated with corresponding enhanced 18F-FDG uptake. This study revealed that PET and ^{13}C DNP-MRS can be used to visualize increased glycolytic flux in malignant tissue. The combined ^{13}C DNP-MRS and PET readouts will allow the quantitative dissection of substrate metabolism, with respect to uptake and downstream metabolic pathways. Nonetheless, these first imaging data suggest the feasibility of 13C MRSI for future clinical use [138].

Integrated PET/MRI measurements for neuroendocrine tumors are not yet available; but efforts have been made by using somatostatin receptor-specific tracer (^{68}Ga-DOTATATE) to improve lesion detection by PET [139]. ^{31}P-MRShas been used to differentiate between responders and nonresponders to arterial embolization in neuroendocrine tumors, with responders that exhibit increased cell membrane renewal (higher phosphomonoester level) and energy consumption (lower NTP and higher Pi levels) [140]. For renal cell carcinoma, ^{1}H-MRS can significantly differentiate tumor from healthy renal parenchyma by comparing their lipid composition [141]. An *in vitro* [1-^{13}C]pyruvate DNP-MRS study of RCC cells showed a significantly higher pyruvate-to-lactate flux than the normal renal tubule cells. These metastatic RCC cells were also found to have significantly higher monocarboxylate transporter 4 (MCT4) expression and corresponding higher lactate efflux than the nonmetastatic cells, which is essential for maintaining a high rate of glycolysis [142].

5. Mass Spectrometry Imaging (MSI)

Mass spectrometry imaging (MSI) is an analytical imaging technique for tissue section. It can provide a very high spatial resolution (typically 10 m) [143], but cannot provide the temporal information as the other noninvasive imaging techniques such as MRS (seconds) and PET (10 seconds to minutes). For spatial mapping, matrix-assisted laser desorption ionization-time of flight (MALDI-TOF) is the most widely used technique to analyze intact biological tissue sections in a two-dimensional fashion [143]. The matrix used in these studies is a small organic molecule with strong absorbance at the laser wavelength. They are applied on the surface of the histological section and cocrystallized with the sample. A laser pulse is used to ionize the chemical compounds on the sample and charged molecules or molecule fragments are then generated. MSI is based on the measurements of the mass-to-charge ratios, which produces spectra to determine the metabolome of the sample. This technique enables the investigation and spatial localization of both identified and unidentified molecules without any need for labeling or contrasting agents, which further facilitates the discovery of new biomarkers and their validation [144]. The damage on the biomedical tissue sections induced by laser irradiation during MALDI-MSI is relatively modest and the histological and biochemical evaluations can be performed on the same tissue slice after the MSI measurements [145] (Figure 3). The combined use of imaging modalities, such as MSI and fluorescent microscopy and histology/immunohistochemistry (IHC) [146] allows metabolic and pathological evaluations of the tissue sections in a highly precise and reliable way. MALDI MSI-based studies have been used to elucidate molecular signatures from samples with different tumor types and grades, including brain [58], oral [59], lung [60], breast [61], gastric [62], pancreatic [63], renal [64], ovarian [65], and prostate cancers [66].

MALDI-MSI is useful for metabolic imaging, albeit the average scanning time might take hours for a single mass image, depending on sample size and resolution. The target for MSI studies limits to lipid molecules of endogenous metabolites because many kinds of matrix ion peaks are observed in the low-mass range ($m/z < 700$), and the strong peaks that they generate interfere with the detection of the target low-molecular-weight compounds. This is because the m/z range of most lipid molecules was more than 700 and also lipids are abundant in tissues (e.g., more than 60% of the dry weight of brain tissue) and are easily ionized because of the presence of a polar head [147, 148]. MALDI-MSI was employed for imaging acylcarnitines, PC, lysophosphatidylcholine (LPC), and sphingomyelin to differentiate viable and necrotic microenvironments of breast tumor xenografts [149]. Recent breakthrough on the use of 9-aminoacridine (9-AA) as a matrix for low-molecular-weight metabolite analysis and negative mode MALDI-MS has been used to detect more than 30 metabolites (which included nucleotides, cofactors, phosphorylated sugars, amino acids, lipids, and carboxylic acids) in ischemia-reperfused rat brain tissue [150]. Hattori et al. have also reported spatiotemporal changes in energy charge, adenylates, and NADH during focal ischemia in a mouse MCAO model [151]. These findings highlight the potential applications of MSI metabolomic imaging technique to visualize spatiodynamics of some aspects of the tissue metabolome.

Although the present MALDI method is highly sensitive and well established on the MSI platform, some limitations need to be overcome before the broad range of endogenous metabolite imaging can be achieved. To date, this method can only apply to *ex vivo* tissue sections. It is generally known that, in MALDI, the detection of molecules is completely dependent on the matrix. In addition, the crystal size of the deposited matrix strongly affects both experimental

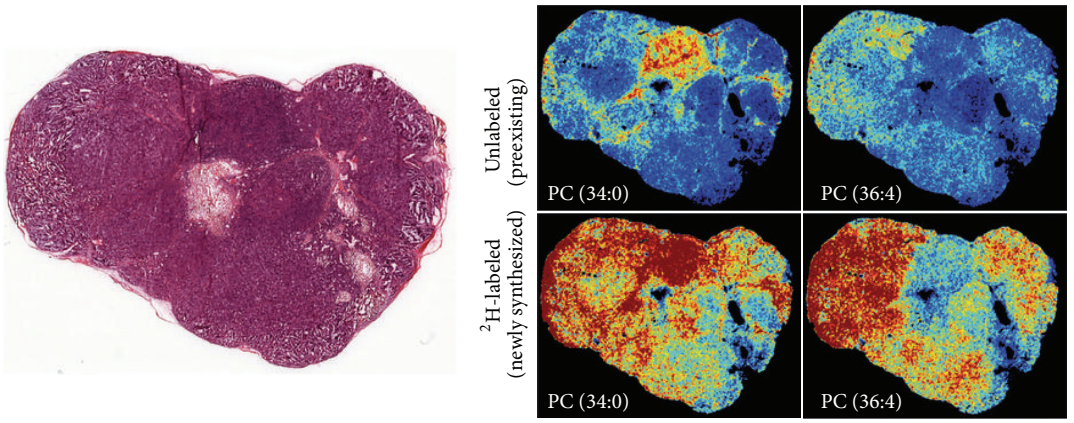

Figure 3: Correlation of histopathology and mass spectrometry imaging. Serial sections of the tumor are used for histopathology (left) correlation with MSI results (right). Deconvolution of spectra is performed to separate 2H-labeled and unlabeled lipids. Intensity images are generated to show the spatial distribution for both newly synthesized and preexisting lipids. Reprinted with permission from [106]. Copyright 2013 Nature Publishing Group, a division of Macmillan Publishers Limited.

reproducibility and spatial resolution in MALDI-MSI. To accelerate the use of MALDI-based metabolic imaging platform, substantial progress in matrix development and its application is required. For tissue imaging in metabolomics, nanostructure-initiator mass spectrometry (NIMS) has been investigated for spatial profiling of metabolites without the need for matrix and with reduced fragmentation [152, 153].

6. Concluding Remarks

The cancer metabolomics information provided by multimodality imaging techniques has revolutionized our ways of cancer treatment. Current oncologic therapy has moved forward from cytotoxic treatment to personalized therapy, such as targeting specific signal pathways or oncogene or metabolic enzymes. This would lead to altering metabolic signatures in tumor tissue, which could be monitored by using MRS or PET imaging. The nonradiation nature of MRS renders its ease of transitioning from bench to bedside. Metabolic information provided by multivoxel MRS measurements combined with the anatomical information provided by MRI can significantly improve the assessment of cancer location and extent and cancer aggressiveness. Biomarkers discovered by MRS can lead to development of new PET tracers. With the development of highly specific molecular probes, DNP-MRS and/or PET will play a major and integral role in the diagnosis, prognosis, and monitoring of treatment response in cancer and other diseases. In combination with classical histological/immunohistochemical methods, MSI analysis can provide new insights into the simultaneously occurring metabolic processes in tissue section that could not be obtained otherwise.

In the future, a combination of *in vivo* noninvasive imaging techniques (MRI anatomic imaging and functional imaging including MRS and PET) in integrated MR/PET scanners and *ex vivo* MSI validation with other tissue analytical platforms, may become the ultimate technology for unraveling and understanding some of the molecular complexities of cancer metabolism. The potential of a comprehensive study on tumor metabolism has recently been demonstrated in a glioma model, by using ^{11}C-choline PET and choline on ^{1}H-MRS for *in vivo* imaging tumors, and tissue MSI for *ex vivo* validation [122]. Such combination might fulfill the function for pharmacometabolomics, biomarker discovery, disease diagnosis and prognosis, and monitoring treatment response. The development of integrated bioinformatics tools would help to handle the spatial, temporal, and multiparametric data from cancer metabolic imaging.

Conflict of Interests

The authors declare that there is no conflict of interests regarding the publication of this paper.

Acknowledgments

We acknowledge the support received from Chang Gung Medical Foundation (Taiwan) Grants CMRPG370444 and CMRPG3B1921, also the Cancer Research UK and EPSRC Cancer Imaging Centre in association with the MRC and Department of Health (England) Grant C1060/A10334.

References

[1] D. Hanahan and R. A. Weinberg, "Hallmarks of cancer: the next generation," *Cell*, vol. 144, no. 5, pp. 646–674, 2011.

[2] R. Kaddurah-Daouk, B. S. Kristal, and R. M. Weinshilboum, "Metabolomics: a global biochemical approach to drug response and disease," *Annual Review of Pharmacology and Toxicology*, vol. 48, pp. 653–683, 2008.

[3] O. Warburg, "On the origin of cancer cells," *Science*, vol. 123, no. 3191, pp. 309–314, 1956.

[4] R. A. Gatenby and R. J. Gillies, "A microenvironmental model of carcinogenesis," *Nature Reviews Cancer*, vol. 8, no. 1, pp. 56–61, 2008.

[5] P. R. Rich, "The molecular machinery of Keilin's respiratory chain," *Biochemical Society Transactions*, vol. 31, no. 6, pp. 1095–1105, 2003.

[6] J. L. Griffin and R. A. Kauppinen, "Tumour metabolomics in animal models of human cancer," *Journal of Proteome Research*, vol. 6, no. 2, pp. 498–505, 2007.

[7] L. C. Costello and R. B. Franklin, "'Why do tumour cells glycolyse?': from glycolysis through citrate to lipogenesis," *Molecular and Cellular Biochemistry*, vol. 280, no. 1-2, pp. 1–8, 2005.

[8] R. L. Elstrom, D. E. Bauer, M. Buzzai et al., "Akt stimulates aerobic glycolysis in cancer cells," *Cancer Research*, vol. 64, no. 11, pp. 3892–3899, 2004.

[9] D. R. Plas and C. B. Thompson, "Akt-dependent transformation: there is more to growth than just surviving," *Oncogene*, vol. 24, no. 50, pp. 7435–7442, 2005.

[10] T. Porstmann, C. R. Santos, B. Griffiths et al., "SREBP activity is regulated by mTORC1 and contributes to Akt-dependent cell growth," *Cell Metabolism*, vol. 8, no. 3, pp. 224–236, 2008.

[11] J.-W. Kim and C. V. Dang, "Cancer's molecular sweet tooth and the warburg effect," *Cancer Research*, vol. 66, no. 18, pp. 8927–8930, 2006.

[12] H. Shim, C. Dolde, B. C. Lewis et al., "c-Myc transactivation of LDH-A: implications for tumor metabolism and growth," *Proceedings of the National Academy of Sciences of the United States of America*, vol. 94, no. 13, pp. 6658–6663, 1997.

[13] J. Downward, "Targeting RAS signalling pathways in cancer therapy," *Nature Reviews Cancer*, vol. 3, no. 1, pp. 11–22, 2003.

[14] S. Telang, A. Yalcin, A. L. Clem et al., "Ras transformation requires metabolic control by 6-phosphofructo-2-kinase," *Oncogene*, vol. 25, no. 55, pp. 7225–7234, 2006.

[15] K. H. Vousden and K. M. Ryan, "P53 and metabolism," *Nature Reviews Cancer*, vol. 9, no. 10, pp. 691–700, 2009.

[16] D. B. Shackelford and R. J. Shaw, "The LKB1-AMPK pathway: metabolism and growth control in tumour suppression," *Nature Reviews Cancer*, vol. 9, no. 8, pp. 563–575, 2009.

[17] K.-K. Wong, J. A. Engelman, and L. C. Cantley, "Targeting the PI3K signaling pathway in cancer," *Current Opinion in Genetics and Development*, vol. 20, no. 1, pp. 87–90, 2010.

[18] N. M. S. Al-Saffar, L. E. Jackson, F. I. Raynaud et al., "The phosphoinositide 3-kinase inhibitor PI-103 downregulates choline kinase α leading to phosphocholine and total choline decrease detected by magnetic resonance spectroscopy," *Cancer Research*, vol. 70, no. 13, pp. 5507–5517, 2010.

[19] N. C. Denko, "Hypoxia, HIF1 and glucose metabolism in the solid tumour," *Nature Reviews Cancer*, vol. 8, no. 9, pp. 705–713, 2008.

[20] M. Beloueche-Babari, L. E. Jackson, N. M. S. Al-Saffar, P. Workman, M. O. Leach, and S. M. Ronen, "Magnetic resonance spectroscopy monitoring of mitogen-activated protein kinase signaling inhibition," *Cancer Research*, vol. 65, no. 8, pp. 3356–3363, 2005.

[21] B. F. Jordan, K. Black, I. F. Robey, M. Runquist, G. Powis, and R. J. Gillies, "Metabolite changes in HT-29 xenograft tumors following HIF-1α inhibition with PX-478 as studied by MR spectroscopy in vivo and ex vivo," *NMR in Biomedicine*, vol. 18, no. 7, pp. 430–439, 2005.

[22] J.-W. Kim, I. Tchernyshyov, G. L. Semenza, and C. V. Dang, "HIF-1-mediated expression of pyruvate dehydrogenase kinase: a metabolic switch required for cellular adaptation to hypoxia," *Cell Metabolism*, vol. 3, no. 3, pp. 177–185, 2006.

[23] N. M. S. Al-Saffar, H. Troy, A. R. de Molina et al., "Noninvasive magnetic resonance spectroscopic pharmacodynamic markers of the choline kinase inhibitor MN58b in human carcinoma models," *Cancer Research*, vol. 66, no. 1, pp. 427–434, 2006.

[24] A. Evans, V. Bates, H. Troy et al., "Glut-1 as a therapeutic target: increased chemoresistance and HIF-1-independent link with cell turnover is revealed through COMPARE analysis and metabolomic studies," *Cancer Chemotherapy and Pharmacology*, vol. 61, no. 3, pp. 377–393, 2008.

[25] P. Sonveaux, T. Copetti, C. J. de Saedeleer et al., "Targeting the lactate transporter MCT1 in endothelial cells inhibits lactate-induced HIF-1 activation and tumor angiogenesis," *PLoS ONE*, vol. 7, no. 3, Article ID e33418, 2012.

[26] R. L. Yauch and J. Settleman, "Recent advances in pathway-targeted cancer drug therapies emerging from cancer genome analysis," *Current Opinion in Genetics and Development*, vol. 22, no. 1, pp. 45–49, 2012.

[27] M. G. Vander Heiden, "Targeting cancer metabolism: a therapeutic window opens," *Nature Reviews Drug Discovery*, vol. 10, no. 9, pp. 671–684, 2011.

[28] D. A. Tennant, R. V. Durán, and E. Gottlieb, "Targeting metabolic transformation for cancer therapy," *Nature Reviews Cancer*, vol. 10, no. 4, pp. 267–277, 2010.

[29] J. Evelhoch, M. Garwood, D. Vigneron et al., "Expanding the use of magnetic resonance in the assessment of tumor response to therapy: workshop report," *Cancer Research*, vol. 65, no. 16, pp. 7041–7044, 2005.

[30] P. Workman, E. O. Aboagye, Y.-L. Chung et al., "Minimally invasive Pharmacokinetic and Pharmacodynamic Technologies in hypothesis-testing clinical trials of innovative therapies," *Journal of the National Cancer Institute*, vol. 98, no. 9, pp. 580–598, 2006.

[31] M. Gerlinger, A. J. Rowan, S. Horswell et al., "Intratumor heterogeneity and branched evolution revealed by multiregion sequencing," *The New England Journal of Medicine*, vol. 366, no. 10, pp. 883–892, 2012.

[32] T. N. Seyfried and L. M. Shelton, "Cancer as a metabolic disease," *Nutrition and Metabolism*, vol. 7, article 7, 2010.

[33] R. A. Gatenby and R. J. Gillies, "Why do cancers have high aerobic glycolysis?" *Nature Reviews Cancer*, vol. 4, no. 11, pp. 891–899, 2004.

[34] M. Israël and L. Schwartz, "The metabolic advantage of tumor cells," *Molecular Cancer*, vol. 10, article 70, 2011.

[35] O. Feron, "Pyruvate into lactate and back: from the Warburg effect to symbiotic energy fuel exchange in cancer cells," *Radiotherapy and Oncology*, vol. 92, no. 3, pp. 329–333, 2009.

[36] P. Icard and H. Lincet, "A global view of the biochemical pathways involved in the regulation of the metabolism of cancer cells," *Biochimica et Biophysica Acta*, vol. 1826, no. 2, pp. 423–433, 2012.

[37] G. L. Semenza, "Tumor metabolism: cancer cells give and take lactate," *The Journal of Clinical Investigation*, vol. 118, no. 12, pp. 3835–3837, 2008.

[38] P. Sonveaux, F. Végran, T. Schroeder et al., "Targeting lactate-fueled respiration selectively kills hypoxic tumor cells in mice," *The Journal of Clinical Investigation*, vol. 118, no. 12, pp. 3930–3942, 2008.

[39] J. L. Griffin and R. A. Kauppinen, "A metabolomics perspective of human brain tumours," *The FEBS Journal*, vol. 274, no. 5, pp. 1132–1139, 2007.

[40] M. G. Swanson, A. S. Zektzer, Z. L. Tabatabai et al., "Quantitative analysis of prostate metabolites using1H HR-MAS spectroscopy," *Magnetic Resonance in Medicine*, vol. 55, no. 6, pp. 1257–1264, 2006.

[41] L. Bartella and W. Huang, "Proton (1H) MR spectroscopy of the breast," *Radiographics*, vol. 27, supplement 1, pp. S241–S252, 2007.

[42] C. Dowling, A. W. Bollen, S. M. Noworolski et al., "Preoperative proton MR spectroscopic imaging of brain tumors: correlation with histopathologic analysis of resection specimens," *American Journal of Neuroradiology*, vol. 22, no. 4, pp. 604–612, 2001.

[43] S. K. Mukherji, S. Schiro, M. Castillo, L. Kwock, K. E. Muller, and W. Blackstock, "Proton MR spectroscopy of squamous cell carcinoma of the extracranial head and neck: in vitro and in vivo studies," *American Journal of Neuroradiology*, vol. 18, no. 6, pp. 1057–1072, 1997.

[44] M. Seitz, A. Shukla-Dave, A. Bjartell et al., "Functional magnetic resonance imaging in prostate cancer," *European Urology*, vol. 55, no. 4, pp. 801–814, 2009.

[45] P. Alusta, I. Im, B. A. Pearce et al., "Improving proton MR spectroscopy of brain tissue for noninvasive diagnostics," *Journal of Magnetic Resonance Imaging*, vol. 32, no. 4, pp. 818–829, 2010.

[46] M. M. Mahon, I. J. Cox, R. Dina et al., "1H Magnetic resonance spectroscopy of preinvasive and invasive cervical cancer: in vivo-ex vivo profiles and effect of tumor load," *Journal of Magnetic Resonance Imaging*, vol. 19, no. 3, pp. 356–364, 2004.

[47] S. J. Nelson, J. Kurhanewicz, D. B. Vigneron et al., "Metabolic imaging of patients with prostate cancer using hyperpolarized [1-13C]pyruvate," *Science Translational Medicine*, vol. 5, no. 198, Article ID 198ra08, 2013.

[48] A. Zhu, D. Lee, and H. Shim, "Metabolic positron emission tomography imaging in cancer detection and therapy response," *Seminars in Oncology*, vol. 38, no. 1, pp. 55–69, 2011.

[49] S.-H. Ng, T.-C. Yen, C.-T. Liao et al., "18F-FDG PET and CT/MRI in oral cavity squamous cell carcinoma: a prospective study of 124 patients with histologic correlation," *Journal of Nuclear Medicine*, vol. 46, no. 7, pp. 1136–1143, 2005.

[50] A. D. van den Abbeele and R. D. Badawi, "Use of positron emission tomography in oncology and its potential role to assess response to imatinib mesylate therapy in gastrointestinal stromal tumors (GISTs)," *European Journal of Cancer*, vol. 38, supplement 5, pp. S60–65, 2002.

[51] S. Stroobants, J. Goeminne, M. Seegers et al., "18FDG-Positron emission tomography for the early prediction of response in advanced soft tissue sarcoma treated with imatinib mesylate (Glivec)," *European Journal of Cancer*, vol. 39, no. 14, pp. 2012–2020, 2003.

[52] N. Sunaga, N. Oriuchi, K. Kaira et al., "Usefulness of FDG-PET for early prediction of the response to gefitinib in non-small cell lung cancer," *Lung Cancer*, vol. 59, no. 2, pp. 203–210, 2008.

[53] B. Simcock, D. Neesham, M. Quinn, E. Drummond, A. Milner, and R. J. Hicks, "The impact of PET/CT in the management of recurrent ovarian cancer," *Gynecologic Oncology*, vol. 103, no. 1, pp. 271–276, 2006.

[54] B. K. P. Goh, "Positron emission tomography/computed tomography influences on the management of resectable pancreatic cancer and its cost-effectiveness," *Annals of Surgery*, vol. 243, no. 5, pp. 709–710, 2006.

[55] H. Schöder, K. Herrmann, M. Gönen et al., "2-[18F]fluoro-2-deoxyglucose positron emission tomography for the detection of disease in patients with prostate-specific antigen relapse after radical prostatectomy," *Clinical Cancer Research*, vol. 11, no. 13, pp. 4761–4769, 2005.

[56] K.-C. Ho, G. Lin, J.-J. Wang, C.-H. Lai, C.-J. Chang, and T.-C. Yen, "Correlation of apparent diffusion coefficients measured by 3T diffusion-weighted MRI and SUV from FDG PET/CT in primary cervical cancer," *European Journal of Nuclear Medicine and Molecular Imaging*, vol. 36, no. 2, pp. 200–208, 2009.

[57] T.-C. Yen, L.-C. See, T.-C. Chang et al., "Defining the priority of using 18F-FDG PET for recurrent cervical cancer," *Journal of Nuclear Medicine*, vol. 45, no. 10, pp. 1632–1639, 2004.

[58] S. A. Schwartz, R. J. Weil, R. C. Thompson et al., "Proteomic-based prognosis of brain tumor patients using direct-tissue matrix-assisted laser desorption ionization mass spectrometry," *Cancer Research*, vol. 65, no. 17, pp. 7674–7681, 2005.

[59] S. A. Patel, A. Barnes, N. Loftus et al., "Imaging mass spectrometry using chemical inkjet printing reveals differential protein expression in human oral squamous cell carcinoma," *The Analyst*, vol. 134, no. 2, pp. 301–307, 2009.

[60] M. R. Groseclose, P. P. Massion, P. Chaurand, and R. M. Caprioli, "High-throughput proteomic analysis of formalin-fixed paraffin-embedded tissue microarrays using MALDI imaging mass spectrometry," *Proteomics*, vol. 8, no. 18, pp. 3715–3724, 2008.

[61] S. Rauser, C. Marquardt, B. Balluff et al., "Classification of HER2 receptor status in breast cancer tissues by MALDI imaging mass spectrometry," *Journal of Proteome Research*, vol. 9, no. 4, pp. 1854–1863, 2010.

[62] Y. Morita, K. Ikegami, N. Goto-Inoue et al., "Imaging mass spectrometry of gastric carcinoma in formalin-fixed paraffin-embedded tissue microarray," *Cancer Science*, vol. 101, no. 1, pp. 267–273, 2010.

[63] M.-C. Djidja, E. Claude, M. F. Snel et al., "MALDI-ion mobility separation-mass spectrometry imaging of glucose-regulated protein 78 kDa (Grp78) in human formalin-fixed, paraffin-embedded pancreatic adenocarcinoma tissue sections," *Journal of Proteome Research*, vol. 8, no. 10, pp. 4876–4884, 2009.

[64] S. R. Oppenheimer, D. Mi, M. E. Sanders, and R. M. Caprioli, "Molecular analysis of tumor margins by MALDI mass spectrometry in renal carcinoma," *Journal of Proteome Research*, vol. 9, no. 5, pp. 2182–2190, 2010.

[65] R. Lemaire, S. A. Menguellet, J. Stauber et al., "Specific MALDI imaging and profiling for biomarker hunting and validation: fragment of the 11S proteasome activator complex, reg alpha fragment, is a new potential ovary cancer biomarker," *Journal of Proteome Research*, vol. 6, no. 11, pp. 4127–4134, 2007.

[66] L. H. Cazares, D. Troyer, S. Mendrinos et al., "Imaging mass spectrometry of a specific fragment of mitogen-activated protein kinase/extracellular signal-regulated kinase kinase kinase 2 discriminates cancer from uninvolved prostate tissue," *Clinical Cancer Research*, vol. 15, no. 17, pp. 5541–5551, 2009.

[67] J. K. Nicholson, J. C. Lindon, and E. Holmes, "'Metabonomics': understanding the metabolic responses of living systems to pathophysiological stimuli via multivariate statistical analysis of biological NMR spectroscopic data," *Xenobiotica*, vol. 29, no. 11, pp. 1181–1189, 1999.

[68] O. Fiehn, J. Kopka, P. Dörmann, T. Altmann, R. N. Trethewey, and L. Willmitzer, "Metabolite profiling for plant functional genomics," *Nature Biotechnology*, vol. 18, no. 11, pp. 1157–1161, 2000.

[69] W. B. Dunn, D. I. Broadhurst, H. J. Atherton, R. Goodacre, and J. L. Griffin, "Systems level studies of mammalian metabolomes:

the roles of mass spectrometry and nuclear magnetic resonance spectroscopy," *Chemical Society Reviews*, vol. 40, no. 1, pp. 387–426, 2011.

[70] E. M. Lenz and I. D. Wilson, "Analytical strategies in metabonomics," *Journal of Proteome Research*, vol. 6, no. 2, pp. 443–458, 2007.

[71] N. Psychogios, D. D. Hau, J. Peng et al., "The human serum metabolome," *PLoS ONE*, vol. 6, no. 2, Article ID e16957, 2011.

[72] J. R. Griffiths and Y. L. Chung, "Metabolomic studies on cancer and on anticancer drugs by NMR ex vivo," in *Encyclopedia of Magnetic Resonance*, R. K. Harris and R. E. Wasylishen, Eds., John Wiley & Sons, Chichester, UK, 2011.

[73] M. V. Brown, J. E. McDunn, P. R. Gunst et al., "Cancer detection and biopsy classification using concurrent histopathological and metabolomic analysis of core biopsies," *Genome Medicine*, vol. 4, no. 4, article 33, 2012.

[74] K. Glunde and Z. M. Bhujwalla, "Metabolic tumor imaging using magnetic resonance spectroscopy," *Seminars in Oncology*, vol. 38, no. 1, pp. 26–41, 2011.

[75] C. P. Slichter, *Principles of Magnetic Resonance*, Springer, New York, NY, USA, 3rd edition, 1990.

[76] J. Frahm, H. Bruhn, M. L. Gyngell, K. D. Merboldt, W. Hanicke, and R. Sauter, "Localized high-resolution proton NMR spectroscopy using stimulated echoes: initial applications to human brain in vivo," *Magnetic Resonance in Medicine*, vol. 9, no. 1, pp. 79–93, 1989.

[77] P. A. Bottomley, "Spatial localization in NMR spectroscopy in vivo," *Annals of the New York Academy of Sciences*, vol. 508, pp. 333–348, 1987.

[78] R. J. Ordidge, R. M. Bowley, and G. McHale, "A general approach to selection of multiple cubic volume elements using the ISIS technique," *Magnetic Resonance in Medicine*, vol. 8, no. 3, pp. 323–331, 1988.

[79] T. R. Brown, B. M. Kincaid, and K. Ugurbil, "NMR chemical shift imaging in three dimensions," *Proceedings of the National Academy of Sciences of the United States of America*, vol. 79, no. 11 I, pp. 3523–3526, 1982.

[80] K. Glunde, C. Jie, and Z. M. Bhujwalla, "Molecalar causes of tile aberrant choline phospholipid metabolism in breast cancer," *Cancer Research*, vol. 64, no. 12, pp. 4270–4276, 2004.

[81] R. J. Gillies and D. L. Morse, "In vivo magnetic resonance spectroscopy in cancer," *Annual Review of Biomedical Engineering*, vol. 7, pp. 287–326, 2005.

[82] J. M. Hakumäki, H. Poptani, A.-M. Sandmair, S. Ylä-Herttuala, and R. A. Kauppinen, "1H MRS detects polyunsaturated fatty acid accumulation during gene therapy of glioma: implications for the in vivo detection of apoptosis," *Nature Medicine*, vol. 5, no. 11, pp. 1323–1327, 1999.

[83] N. M. S. Al-Saffar, J. C. Titley, D. Robertson et al., "Apoptosis is associated with triacylglycerol accumulation in Jurkat T-cells," *British Journal of Cancer*, vol. 86, no. 6, pp. 963–970, 2002.

[84] J. E. Schmitz, M. I. Kettunen, D.-E. Hu, and K. M. Brindle, "1H MRS-visible lipids accumulate during apoptosis of lymphoma cells in vitro and in vivo," *Magnetic Resonance in Medicine*, vol. 54, no. 1, pp. 43–50, 2005.

[85] J. L. Griffin, K. K. Lehtimäki, P. K. Valonen et al., "Assignment of 1H nuclear magnetic resonance visible polyunsaturated fatty acids in BT4C gliomas undergoing ganciclovir-thymidine kinase gene therapy-induced programmed cell death," *Cancer Research*, vol. 63, no. 12, pp. 3195–3201, 2003.

[86] P. G. Okunieff, J. A. Koutcher, L. Gerweck et al., "Tumor size dependent changes in a murine fibrosarcoma: use of in vivo 31P NMR for non-invasive evaluation of tumor metabolic status," *International Journal of Radiation Oncology Biology Physics*, vol. 12, no. 5, pp. 793–799, 1986.

[87] G. M. Tozer and J. R. Griffiths, "The contribution made by cell death and oxygenation to 31P MRS observations of tumour energy metabolism," *NMR in Biomedicine*, vol. 5, no. 5, pp. 279–289, 1992.

[88] W. Wolf, C. A. Presant, and V. Waluch, "19F-MRS studies of fluorinated drugs in humans," *Advanced Drug Delivery Reviews*, vol. 41, no. 1, pp. 55–74, 2000.

[89] Y.-L. Chung, H. Troy, I. R. Judson et al., "Noninvasive measurements of capecitabine metabolism in bladder tumors overexpressing thymidine phosphorylase by fluorine-19 magnetic resonance spectroscopy," *Clinical Cancer Research*, vol. 10, no. 11, pp. 3863–3870, 2004.

[90] C. Li, M.-F. Penet, P. Winnard Jr., D. Artemov, and Z. M. Bhujwalla, "Image-guided enzyme/prodrug cancer therapy," *Clinical Cancer Research*, vol. 14, no. 2, pp. 515–522, 2008.

[91] E. L. Hall, M. C. Stephenson, D. Price, and P. G. Morris, "Methodology for improved detection of low concentration metabolites in MRS: optimised combination of signals from multi-element coil arrays," *NeuroImage*, vol. 86, pp. 35–42, 2014.

[92] J. H. Ardenkjær-Larsen, B. Fridlund, A. Gram et al., "Increase in signal-to-noise ratio of >10,000 times in liquid-state NMR," *Proceedings of the National Academy of Sciences of the United States of America*, vol. 100, no. 18, pp. 10158–10163, 2003.

[93] D. M. Wilson, K. R. Keshari, P. E. Z. Larson et al., "Multi-compound polarization by DNP allows simultaneous assessment of multiple enzymatic activities in vivo," *Journal of Magnetic Resonance*, vol. 205, no. 1, pp. 141–147, 2010.

[94] T. H. Witney, M. I. Kettunen, D.-E. Hu et al., " Detecting treatment response in a model of human breast adenocarcinoma using hyperpolarised [1-13C]pyruvate and [1,4-13C2]fumarate," *British Journal of Cancer*, vol. 103, no. 9, pp. 1400–1406, 2010.

[95] K. Golman, R. I. Zandt, M. Lerche, R. Pehrson, and J. H. Ardenkjaer-Larsen, "Metabolic imaging by hyperpolarized ^{13}C magnetic resonance imaging for in vivo tumor diagnosis," *Cancer Research*, vol. 66, no. 22, pp. 10855–10860, 2006.

[96] J. Kurhanewicz, D. B. Vigneron, K. Brindle et al., "Analysis of cancer metabolism by imaging hyperpolarized nuclei: prospects for translation to clinical research," *Neoplasia*, vol. 13, no. 2, pp. 81–97, 2011.

[97] S. E. Day, M. I. Kettunen, F. A. Gallagher et al., "Detecting tumor response to treatment using hyperpolarized ^{13}C magnetic resonance imaging and spectroscopy," *Nature Medicine*, vol. 13, no. 11, pp. 1382–1387, 2007.

[98] A. P. Chen, W. Chu, Y. P. Gu, and C. H. Cunnhingham, "Probing early tumor response to radiation therapy using hyperpolarized [1-(1)(3)C]pyruvate in MDA-MB-231 xenografts," *PLoS ONE*, vol. 8, no. 2, Article ID e56551, 2013.

[99] I. Park, R. Bok, T. Ozawa et al., "Detection of early response to temozolomide treatment in brain tumors using hyperpolarized ^{13}C MR metabolic imaging," *Journal of Magnetic Resonance Imaging*, vol. 33, no. 6, pp. 1284–1290, 2011.

[100] C. S. Ward, H. S. Venkatesh, M. M. Chaumeil et al., "Noninvasive detection of target modulation following phosphatidylinositol 3-kinase inhibition using hyperpolarized ^{13}C magnetic resonance spectroscopy," *Cancer Research*, vol. 70, no. 4, pp. 1296–1305, 2010.

[101] K. Golman, L. E. Olsson, O. Axelsson, S. Månsson, M. Karlsson, and J. S. Petersson, "Molecular imaging using hyperpolarized ^{13}C," *The British Journal of Radiology*, vol. 76, no. 2, pp. S118–S127, 2003.

[102] D. K. Hill, Y. Jamin, M. R. Orton et al., "(1)H NMR and hyperpolarized (1)(3)C NMR assays of pyruvate-lactate: a comparative study," *NMR in Biomedicine*, vol. 26, no. 10, pp. 1321–1325, 2013.

[103] D. K. Hill, M. R. Orton, E. Mariotti et al., "Model free approach to kinetic analysis of real-time hyperpolarized ^{13}C magnetic resonance spectroscopy data," *PLoS ONE*, vol. 8, no. 9, Article ID e71996, 2013.

[104] F. A. Gallagher, M. I. Kettunen, S. E. Day et al., "Magnetic resonance imaging of pH in vivo using hyperpolarized ^{13}C-labelled bicarbonate," *Nature*, vol. 453, no. 7197, pp. 940–943, 2008.

[105] F. A. Gallagher, M. I. Kettunen, D.-E. Hu et al., "Production of hyperpolarized [1,4-13C2]malate from [1,4-13C2]fumarate is a marker of cell necrosis and treatment response in tumors," *Proceedings of the National Academy of Sciences of the United States of America*, vol. 106, no. 47, pp. 19801–19806, 2009.

[106] S. J. Nelson, J. Kurhanewicz, D. B. Vigneron et al., "Metabolic imaging of patients with prostate cancer using hyperpolarized [1-(1)(3)C]pyruvate," *Science Translational Medicine*, vol. 5, no. 198, Article ID 198ra08, 2013.

[107] V. Kapoor, B. M. McCook, and F. S. Torok, "An introduction to PET-CT imaging," *Radiographics*, vol. 24, no. 2, pp. 523–543, 2004.

[108] M. L. Macheda, S. Rogers, and J. D. Best, "Molecular and cellular regulation of glucose transporter (GLUT) proteins in cancer," *Journal of Cellular Physiology*, vol. 202, no. 3, pp. 654–662, 2005.

[109] S. Maschauer, O. Prante, M. Hoffmann, J. T. Deichen, and T. Kuwert, "Characterization of 18F-FDG uptake in human endothelial cells in vitro," *Journal of Nuclear Medicine*, vol. 45, no. 3, pp. 455–460, 2004.

[110] K. A. Wood, P. J. Hoskin, and M. I. Saunders, "Positron emission tomography in oncology: a review," *Clinical Oncology*, vol. 19, no. 4, pp. 237–255, 2007.

[111] C. Plathow and W. A. Weber, "Tumor cell metabolism imaging," *Journal of Nuclear Medicine*, vol. 49, supplement 2, pp. 43S–63S, 2008.

[112] I. Grassi, C. Nanni, V. Allegri et al., "The clinical use of PET with (11)C-acetate," *American Journal of Nuclear Medicine and Molecular Imaging*, vol. 2, no. 1, pp. 33–47, 2012.

[113] A. W. Glaudemans, R. H. Enting, M. A. Heesters et al., "Value of 11C-methionine PET in imaging brain tumours and metastases," *European Journal of Nuclear Medicine and Molecular Imaging*, vol. 40, no. 4, pp. 615–635, 2013.

[114] D. Hausmann, L. K. Bittencourt, U. I. Attenberger et al., "Diagnostic accuracy of 18F choline PET/CT using time-of-flight reconstruction algorithm in prostate cancer patients with biochemical recurrence," *Clinical Nuclear Medicine*, 2013.

[115] D. Soloviev, D. Lewis, D. Honess, and E. Aboagye, "[18F]FLT: an imaging biomarker of tumour proliferation for assessment of tumour response to treatment," *European Journal of Cancer*, vol. 48, no. 4, pp. 416–424, 2012.

[116] V. Paolillo, H. H. Yeh, U. Mukhopadhyay, J. G. Gelovani, and M. M. Alauddin, "Improved detection and measurement of low levels of [18F]fluoride metabolized from [18F]-labeled pyrimidine nucleoside analogues in biological samples," *Nuclear Medicine and Biology*, vol. 38, no. 8, pp. 1129–1134, 2011.

[117] F. A. Gallagher, S. E. Bohndiek, M. I. Kettunen, D. Y. Lewis, D. Soloviev, and K. M. Brindle, "Hyperpolarized^{13}C MRI and PET: in vivo tumor biochemistry," *Journal of Nuclear Medicine*, vol. 52, no. 9, pp. 1333–1336, 2011.

[118] J. Culver, W. Akers, and S. Achilefu, "Multimodality molecular imaging with combined optical and SPECT/PET modalities," *Journal of Nuclear Medicine*, vol. 49, no. 2, pp. 169–172, 2008.

[119] M. J. Albers, R. Bok, A. P. Chen et al., "Hyperpolarized 13C lactate, pyruvate, and alanine: noninvasive biomarkers for prostate cancer detection and grading," *Cancer Research*, vol. 68, no. 20, pp. 8607–8615, 2008.

[120] C. Buchbender, T. A. Heusner, T. C. Lauenstein, A. Bockisch, and G. Antoch, "Oncologic PET/MRI, part 1: tumors of the brain, head and neck, chest, abdomen, and pelvis," *Journal of Nuclear Medicine*, vol. 53, no. 6, pp. 928–938, 2012.

[121] S. E. Bohndiek and K. M. Brindle, "Imaging and 'omic methods for the molecular diagnosis of cancer," *Expert Review of Molecular Diagnostics*, vol. 10, no. 4, pp. 417–434, 2010.

[122] H. F. Wehrl, J. Schwab, K. Hasenbach et al., "Multimodal elucidation of choline metabolism in a murine glioma model using magnetic resonance spectroscopy and ^{11}C-choline positron emission tomography," *Cancer Research*, vol. 73, no. 5, pp. 1470–1480, 2013.

[123] T. A. Smith, M. V. Appleyard, S. Sharp, I. N. Fleming, K. Murray, and A. M. Thompson, "Response to trastuzumab by HER2 expressing breast tumour xenografts is accompanied by decreased Hexokinase II, glut1 and [18F]-FDG incorporation and changes in 31P-NMR-detectable phosphomonoesters," *Cancer Chemotherapy and Pharmacology*, vol. 71, no. 2, pp. 473–480, 2013.

[124] W. Wolf, "The unique potential for noninvasive imaging in modernizing drug development and in transforming therapeutics: PET/MRI/MRS," *Pharmaceutical Research*, vol. 28, no. 3, pp. 490–493, 2011.

[125] J. F. A. Jansen, H. Schöder, N. Y. Lee et al., "Tumor metabolism and perfusion in head and neck squamous cell carcinoma: pretreatment multimodality imaging with1H magnetic resonance spectroscopy, dynamic contrast-enhanced MRI, and [18F]FDG-PET," *International Journal of Radiation Oncology Biology Physics*, vol. 82, no. 1, pp. 299–307, 2012.

[126] C. Testa, R. Schiavina, R. Lodi et al., "Prostate cancer: sextant localization with MR imaging, MR spectroscopy, and 11C-choline PET/CT," *Radiology*, vol. 244, no. 3, pp. 797–806, 2007.

[127] V. Panebianco, A. Sciarra, D. Lisi et al., "Prostate cancer: 1HMRS-DCEMR at 3 T versus [(18)F]choline PET/CT in the detection of local prostate cancer recurrence in men with biochemical progression after radical retropubic prostatectomy (RRP)," *European Journal of Radiology*, vol. 81, no. 4, pp. 700–708, 2012.

[128] M. Tozaki and K. Hoshi, "1H MR spectroscopy of invasive ductal carcinoma: correlations with FDG PET and histologic prognostic factors," *American Journal of Roentgenology*, vol. 194, no. 5, pp. 1384–1390, 2010.

[129] R. Katz-Brull, P. T. Lavin, and R. E. Lenkinski, "Clinical utility of proton magnetic resonance spectroscopy in characterizing breast lesions," *Journal of the National Cancer Institute*, vol. 94, no. 16, pp. 1197–1203, 2002.

[130] A. Kumiko, I. Reiichi, N. Yuki et al., "Usefulness of Cho/Cr ratio in proton MR spectroscopy for differentiating residual/recurrent glioma from non-neoplastic lesions," *Nippon Acta Radiologica*, vol. 64, no. 3, pp. 121–126, 2004.

[131] R. Hourani, L. J. Brant, T. Rizk, J. D. Weingart, P. B. Barker, and A. Horská, "Can proton MR spectroscopic and perfusion imaging differentiate between neoplastic and nonneoplastic brain lesions in adults?" *American Journal of Neuroradiology*, vol. 29, no. 2, pp. 366–372, 2008.

[132] E. A. Smith, R. C. Carlos, L. R. Junck, C. I. Tsien, A. Elias, and P. C. Sundgren, "Developing a clinical decision model: MR spectroscopy to differentiate between recurrent tumor and radiation change in patients with new contrast-enhancing lesions," *American Journal of Roentgenology*, vol. 192, no. 2, pp. W45–W52, 2009.

[133] S. A. Sung, M.-J. Kim, S. L. Joon, H.-S. Hong, E. C. Yong, and J.-Y. Choi, "Added value of gadoxetic acid-enhanced hepatobiliary phase MR imaging in the diagnosis of hepatocellular carcinoma," *Radiology*, vol. 255, no. 2, pp. 459–466, 2010.

[134] J. Hwang, S. H. Kim, M. W. Lee, and J. Y. Lee, "Small, (≤ = 2 cm) hepatocellular carcinoma in patients with chronic liver disease: comparison of gadoxetic acid-enhanced 3.0 T MRI and multiphasic 64-multirow detector CT," *The The British Journal of Radiology*, vol. 85, no. 1015, pp. e314–e322, 2012.

[135] M. J. Park, Y. K. Kim, M. W. Lee et al., "Small hepatocellular carcinomas: improved sensitivity by combining gadoxetic acid-enhanced and diffusion-weighted MR imaging patterns," *Radiology*, vol. 264, no. 3, pp. 761–770, 2012.

[136] J.-W. Park, H. K. Ji, K. K. Seok et al., "A prospective evaluation of18F-FDG and11C-acetate PET/CT for detection of primary and metastatic hepatocellular carcinoma," *Journal of Nuclear Medicine*, vol. 49, no. 12, pp. 1912–1921, 2008.

[137] J.-N. Talbot, L. Fartoux, S. Balogova et al., "Detection of hepatocellular carcinoma with PET/CT: a prospective comparison of18F-fluorocholine and18F-FDG in patients with cirrhosis or chronic liver disease," *Journal of Nuclear Medicine*, vol. 51, no. 11, pp. 1699–1706, 2010.

[138] M. I. Menzel, E. V. Farrell, M. A. Janich et al., "Multimodal assessment of in vivo metabolism with hyperpolarized [1-13C]MR spectroscopy and 18F-FDG PET imaging in hepatocellular carcinoma tumor-bearing rats," *Journal of Nuclear Medicine*, vol. 54, no. 7, pp. 1113–1119, 2013.

[139] R. Srirajaskanthan, I. Kayani, A. M. Quigley, J. Soh, M. E. Caplin, and J. Bomanji, "The role of 68Ga-DOTATATE PET in patients with neuroendocrine tumors and negative or equivocal findings on 111In-DTPA-octreotide scintigraphy," *Journal of Nuclear Medicine*, vol. 51, no. 6, pp. 875–882, 2010.

[140] M. Ljungberg, G. Westberg, B. Vikhoff-Baaz et al., "31P MR spectroscopy to evaluate the efficacy of hepatic artery embolization in the treatment of neuroendocrine liver metastases," *Acta Radiologica*, vol. 53, no. 10, pp. 1118–1126, 2012.

[141] F. Sullentrop, J. Hahn, and D. Moka, "In vitro and in vivo (1)H-MR spectroscopic examination of the renal cell carcinoma," *International Journal of Biomedical Science*, vol. 8, no. 2, pp. 94–108, 2012.

[142] K. R. Keshari, R. Sriram, B. L. Koelsch et al., "Hyperpolarized 13C-pyruvate magnetic resonance reveals rapid lactate export in metastatic renal cell carcinomas," *Cancer Research*, vol. 73, no. 2, pp. 529–538, 2013.

[143] D. S. Cornett, J. A. Mobley, E. C. Dias et al., "A novel histology-directed strategy for MALDI-MS tissue profiling that improves throughput and cellular specificity in human breast cancer," *Molecular and Cellular Proteomics*, vol. 5, no. 10, pp. 1975–1983, 2006.

[144] S. Nimesh, S. Mohottalage, R. Vincent, and P. Kumarathasan, "Current status and future perspectives of mass spectrometry imaging," *International Journal of Molecular Sciences*, vol. 14, no. 6, pp. 11277–11301, 2013.

[145] D. Miura, Y. Fujimura, and H. Wariishi, "In situ metabolomic mass spectrometry imaging: recent advances and difficulties," *Journal of Proteomics*, vol. 75, no. 16, pp. 5052–5060, 2012.

[146] A. C. Crecelius, D. S. Cornett, R. M. Caprioli, B. Williams, B. M. Dawant, and B. Bodenheimer, "Three-dimensional visualization of protein expression in mouse brain structures using imaging mass spectrometry," *Journal of the American Society for Mass Spectrometry*, vol. 16, no. 7, pp. 1093–1099, 2005.

[147] T. Harada, A. Yuba-Kubo, Y. Sugiura et al., "Visualization of volatile substances in different organelles with an atmospheric-pressure mass microscope," *Analytical Chemistry*, vol. 81, no. 21, pp. 9153–9157, 2009.

[148] G. Sun, K. Yang, Z. Zhao, S. Guan, X. Han, and R. W. Gross, "Matrix-assisted laser desorption/ionization time-of-flight mass spectrometric analysis of cellular glycerophospholipids enabled by multiplexed solvent dependent analyte-matrix interactions," *Analytical Chemistry*, vol. 80, no. 19, pp. 7576–7585, 2008.

[149] K. Chughtai, L. Jiang, T. R. Greenwood, K. Glunde, and R. M. Heeren, "Mass spectrometry images acylcarnitines, phosphatidylcholines, and sphingomyelin in MDA-MB-231 breast tumor models," *Journal of Lipid Research*, vol. 54, no. 2, pp. 333–344, 2013.

[150] D. Miura, Y. Fujimura, M. Yamato et al., "Ultrahighly sensitive in situ metabolomic imaging for visualizing spatiotemporal metabolic behaviors," *Analytical Chemistry*, vol. 82, no. 23, pp. 9789–9796, 2010.

[151] K. Hattori, M. Kajimura, T. Hishiki et al., "Paradoxical ATP elevation in ischemic penumbra revealed by quantitative imaging mass spectrometry," *Antioxidants and Redox Signaling*, vol. 13, no. 8, pp. 1157–1167, 2010.

[152] R. Calavia, F. E. Annanouch, X. Correig, and O. Yanes, "Nanostructure Initiator Mass Spectrometry for tissue imaging in metabolomics: future prospects and perspectives," *Journal of Proteomics*, vol. 75, no. 16, pp. 5061–5068, 2012.

[153] T. R. Northen, O. Yanes, M. T. Northen et al., "Clathrate nanostructures for mass spectrometry," *Nature*, vol. 449, no. 7165, pp. 1033–1036, 2007.

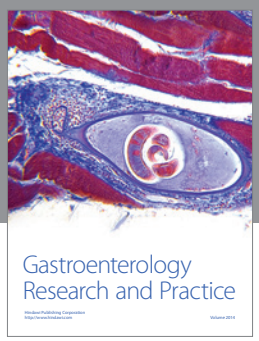

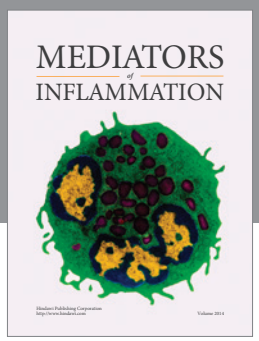

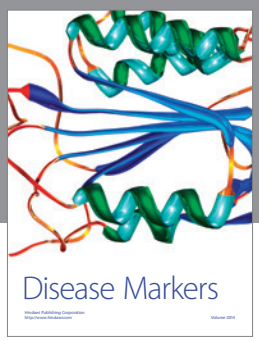

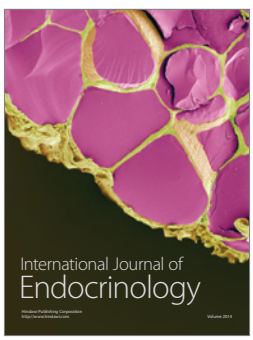

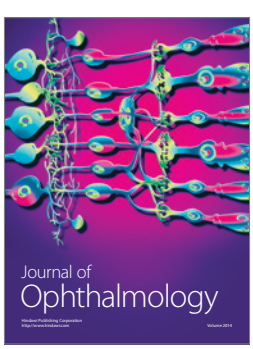

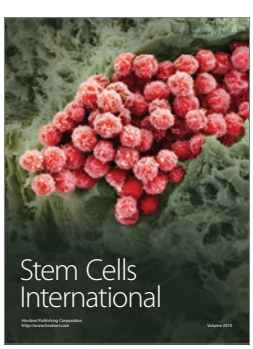

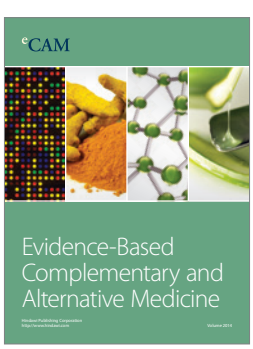

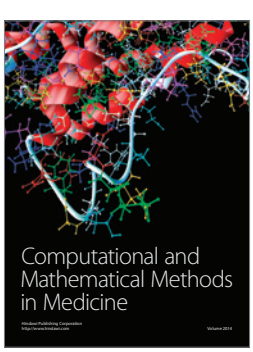

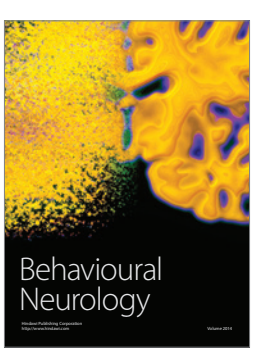

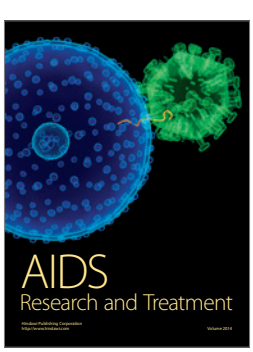

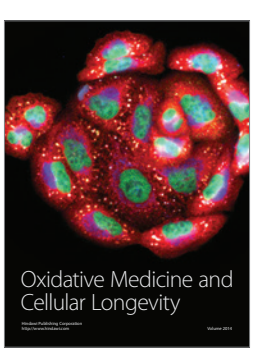

Hindawi

Submit your manuscripts at
http://www.hindawi.com